THE JOURNAL OF PHYSICAL CHEMISTRY B

Article

Cite This: J. Phys. Chem. B 2019, 123, 3079−3085

pubs.acs.org/JPCB

Intramolecular Fluorescent Protein Association in a Class of Zinc FRET Sensors Leads to Increased Dynamic Range

Joshua D. Slocum,[†] Amy E. Palmer,[‡,§] and Ralph Jimenez*[,†,∥]

[†]JILA, University of Colorado and National Institute of Standards and Technology, Boulder, Colorado 80309, United States

[‡]Department of Biochemistry, [§]BioFrontiers Institute, and [∥]Department of Chemistry, University of Colorado, Boulder, Colorado 80309, United States

Supporting Information

ABSTRACT: Genetically encoded Förster resonance energy transfer (FRET) sensors enable the visualization of ions, molecules, and processes in live cells. However, despite their widespread use, the molecular states that determine sensor performance are usually poorly understood, which limits efforts to improve them. We used dynamic light scattering (DLS) and time-resolved fluorescence anisotropy to uncover the sensing mechanism of ZifCV1.173, a Zn^{2+} FRET sensor. We found that the dynamic range (DR) of ZifCV1.173 was dominated by the high FRET efficiency of the Zn^{2+}-free state, in which the donor and acceptor fluorescent proteins were closely associated. Mutating the donor−acceptor interface revealed that the DR of ZifCV1.173 could be increased or decreased by promoting or disrupting the donor−acceptor interaction, respectively. Adapting the same mutations to a related sensor showed the same pattern of DR tuning, supporting our sensing mechanism and suggesting that DLS and time-resolved fluorescence anisotropy might be generally useful in the biophysical characterization of other FRET sensors.

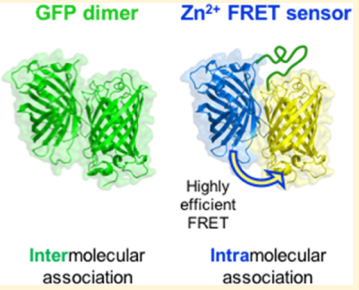

INTRODUCTION

Genetically encoded Förster resonance energy transfer (FRET) sensors are widely used to track the localization and dynamics of biological ions and molecules in live cells. These sensors consist of donor and acceptor fluorescent protein (FP) domains (often cyan- and yellow-emitting variants, respectively) attached to a structurally responsive analyte binding domain. The resulting macromolecule is capable of converting a binding event into a change in FRET efficiency between the donor and acceptor FP domains, which can be imaged and related to the analyte concentration. Thanks to the ease of modern cloning techniques and the availability of analyte binding domain crystal structures to guide their design, there are currently over 100 analytes[1] for which a genetically encoded FRET sensor exists, including many ions[2−7] and small molecules.[8,9]

Despite the well-known dependence of FRET on the distance and orientation between donor and acceptor transition dipole moments,[10] as well as the availability of structural information for the individual sensor components, there is often little-to-no understanding of the underlying molecular configurations that give rise to sensor response. Furthermore, FRET sensors often perform poorly and require optimization to be useful. However, in the absence of specific molecular information, optimization efforts are usually limited to modifications of linker and FP domains that are borrowed from fundamentally different sensors.[9,11,12] Although these efforts do often result in improved sensors, the lack of molecular insight into the sensing process limits the development of new sensors and the improvement of existing ones.

We set out to characterize the molecular states involved in the FRET response to Zn^{2+} binding for a class of Zn^{2+} FRET sensors (Figure 1) that consist of enhanced cyan fluorescent

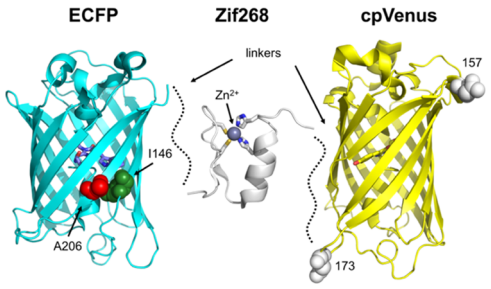

Figure 1. Components of the Zn^{2+} FRET sensor, ZifCV1.173. The crystal structures of enhanced cyan fluorescent protein (ECFP) (cyan, pdb: 2wsn) and Venus (yellow, pdb: 1myw) are shown as ribbons, with the mutation sites (A206 and I146 on ECFP) and circular permutation sites (157 and 173 on Venus) shown as spheres. A single Zn^{2+} finger from the Zif268 transcription factor makes up the Zn^{2+} binding domain (ZBD) and is shown in gray (pdb: 1p47) with bound Zn^{2+} shown as a dark gray sphere coordinated by two cysteine and two histidine residues. Three amino acids link the Zn^{2+} finger to either FP and are represented as dashed lines. In ZifCV1.157, the Venus domain is linked to the rest of the sensor at position 157, giving the donor and acceptor domains a different relative orientation.

Received: March 15, 2019
Revised: March 21, 2019
Published: April 3, 2019

DOI: 10.1021/acs.jpcb.9b02479
J. Phys. Chem. B 2019, 123, 3079−3085

protein (ECFP)[13] and Venus[14] connected by a Zn^{2+} finger from the yeast transcription factor, Zif268.[15] This class of Zn^{2+} sensors was designed by Dittmer et al. on the basis that the Zif268 Zn^{2+} fingers are unstructured in the absence of Zn^{2+} and adopt a helix-β-hairpin fold (Figure 1, gray) upon binding to Zn^{2+}.[16] Park et al. used circular permutations of Venus to improve the sensor dynamic ranges (DR),[17] which is defined as the magnitude of the FRET change in response to analyte binding

$$\mathrm{DR} = \frac{R_{\max}}{R_{\min}} \tag{1}$$

where R_{max} and R_{min} are the maximum and minimum ratios, respectively, of acceptor to donor fluorescence, upon donor excitation. The DR of any sensor is, therefore, a reflection of the change in FRET efficiency that results from analyte binding and is due to altered distance and/or orientation between donor and acceptor FPs. One promising variant, ZifCV1.173, contains cpVenus173 as the FRET acceptor and showed a DR of 2.6 in the mitochondria of HeLa cells, which allowed for a more accurate quantification of mitochondrial Zn^{2+} compared to the first-generation sensor which had a DR of 1.2.[17]

We used a combination of time-resolved fluorescence anisotropy and dynamic light scattering (DLS) to measure the configurational changes that accompany Zn^{2+} binding to ZifCV1.173 in vitro. Our results suggest a sensing mechanism whereby the FP domains of ZifCV1.173 are engaged in close intramolecular association in the absence of Zn^{2+}, in an orientation that resembles the homodimer complex of green fluorescent protein (GFP). The close association of ECFP and cpVenus173 leads to efficient FRET in this state. Binding of Zn^{2+} causes a large change in both the separation and relative orientation of ECFP and cpVenus173, leading to a drastic reduction in FRET efficiency and an overall high DR. Mutations to the interface between ECFP and cpVenus173 allowed us to rationally tune the sensor DR by manipulating the strength of the intramolecular FP association, including the I146N mutation which nearly tripled the DR of ZifCV1.173 and the closely related ZifCV1.157. Our success in tuning sensor performance lends support to our hypothesized sensing mechanism and suggests that the I146N mutation could be used to improve the DR of FRET sensors that operate via a similar mechanism. Indeed, the formation of a compact state with close donor−acceptor FP domain interactions has been engineered into several different FRET sensor platforms and is a powerful strategy for increasing sensor DR.[7,18−20] However, to our knowledge, the I146N mutation has not previously been used to improve the DR of a FRET sensor. Additionally, the combination of time-resolved fluorescence anisotropy and DLS will undoubtedly prove useful in engineering efforts of FRET sensors in general.

EXPERIMENTAL METHODS

Expression and Purification of Sensors. The genes for His_6-tagged ZifCV1.173 and ZifCV1.157 were introduced into pBAD vectors between the *Bam*HI and *Eco*RI restriction sites, and mutations were made to positions 146 and 206 using a QuickChange mutagenesis kit from Agilent with primers carrying the desired mutations (see the Supporting Information for full DNA sequences). pBAD vectors containing the desired sequence were used to transform Top10 *Escherichia coli* cells, which were grown overnight at 37 °C on agarose plates containing ampicillin. Single colonies were picked and grown for 12−16 h at 37 °C in 5 mL of lysogeny broth, shaking at 250 rpm. These starter cultures (1 mL of the 5 mL culture) were used to seed the growth of 400−800 mL of culture. Sensors were expressed for 24−36 h at 28 °C with the addition of 0.2% arabinose (w/v) after the cultures reached an OD of 0.6. Cells were harvested by centrifugation at 5500*g* for 15 min and frozen at −80 °C for at least 2 h before thawing at 4 °C. Thawed cells were treated with 3 mL of bacterial protein extraction reagent (Thermo) per gram of dry cell pellet (typically 1−2 g) at room temperature while stirring for at least 30 min, and then the His_6-tagged sensors were purified via nickel−nitrilotriacetic acid (Ni−NTA) chromatography. Eluted His_6-tagged sensors were buffer exchanged to a buffer containing 20 mM *N*-(2-hydroxyethyl)piperazine-*N*′-ethanesulfonic acid (Hepes), 100 mM NaCl, 1 mM dithiothreitol (DTT), and 20 μM $ZnCl_2$ at pH 8, concentrated to 1 mg/mL, and then subjected to proteolysis by His-TEV (Sigma) at a molar ratio of 1:50 (His-TEV/sensor) for 12−16 h at 4°C. Cleaved sensors were purified using Ni−NTA chromatography, treated with 1 mM ethylenediaminetetraacetic acid (EDTA) for 30−60 min to remove any free or bound Zn^{2+}, and then were buffer exchanged to a buffer containing 1 mM DTT, 150 mM Hepes, and 100 mM NaCl at pH 7.4 in chelex-treated water. Typical sensor yields were 5−10 mg from 800 mL of the culture. Purified sensors were used immediately or were flash frozen in liquid nitrogen and stored at −80 °C.

Dynamic Light Scattering and Fluorescence Anisotropy. For DLS measurements, purified sensor was concentrated to ∼8 μM and incubated for at least 5 min with a buffered Zn^{2+} solution, prepared as described previously,[6] to a final Zn^{2+} concentration of 20 μM to ensure complete saturation of the sensor. DLS spectra were collected using a Malvern Zetasizer, averaging 3 runs per sample, with at least 12 scans per run. Reported hydrodynamic diameters are averaged from at least three technical replicates. After recording the data for the saturated Zn^{2+} conditions, samples were incubated with 1 mM EDTA for at least 5 min before recording the data exactly as before. A FluoTime 100 time-correlated single photon counting spectrometer was used to record time-resolved fluorescence decays with TimeHarp 260 timing electronics. A 440 nm pulsed laser (PicoQuant; pulse width < 200 ps) operating at a repetition frequency of 20 MHz was used to excite the samples. Emission was collected using a PMA 200 photomultiplier tube (PicoQuant) after passing through either donor or acceptor bandpass filters (donor: 480 ± 30 nm; acceptor: 542 ± 27 nm). Purified sensors were concentrated to ∼1 μM and mixed with a 12 μM buffered Zn^{2+} solution prepared, as described previously.[6] Samples were incubated for at least 5 min to ensure that the sensors were fully saturated during measurements. Using vertically polarized excitation, decays were recorded with both vertically and horizontally polarized emission in both the donor and acceptor channels, with at least three technical replicates of each decay recorded per sensor. After recording decays in the saturating Zn^{2+} conditions, the sensors were incubated with 1 mM EDTA for at least 5 min before recording all decays exactly as before.

Zn^{2+} Sensor Titrations. Sensor titrations were performed by diluting purified sensor to a final concentration of 1 μM in a buffer containing 1 mM DTT, 150 mM Hepes, 100 mM NaCl, and the desired concentration of buffered Zn^{2+} (prepared as described previously[6]) at pH 7.4 in chelex-treated water. After incubation for at least 5 min, 100 μL of the sensor/Zn^{2+}

DOI: 10.1021/acs.jpcb.9b02479
J. Phys. Chem. B 2019, 123, 3079−3085

solution was added to the wells of a black round-bottom 96-well plate. The fluorescence intensities at 485 and 531 nm under 440 nm excitation were recorded using a Molecular Devices ID3 plate reader. Plots of the ratio of 531 to 485 nm fluorescence vs Zn^{2+} concentration were fit in Matlab using the model defined by eq 2 and described in detail by Pomorski and co-workers[21]

$$R = \frac{I_{531,B}\cdot[Zn^{2+}]^n + I_{531,U}\cdot[K_D]^n}{I_{485,B}\cdot[Zn^{2+}]^n + I_{485,U}\cdot[K_D]^n} \quad (2)$$

where I_{531} and I_{485} are the fluorescence intensities at 531 and 485 nm, respectively, $[Zn^{2+}]$ is the concentration of buffered Zn^{2+}, K_D is the apparent Zn^{2+} affinity, n is the Hill coefficient, and the subscripts U and B represent the unbound and bound states of the sensor, respectively.

RESULTS AND DISCUSSION

We purified ZifCV1.173 from *E. coli* and characterized its properties in the presence of Zn^{2+} and EDTA, a strong metal chelator. Figure 2A shows emission spectra of ZifCV1.173 in

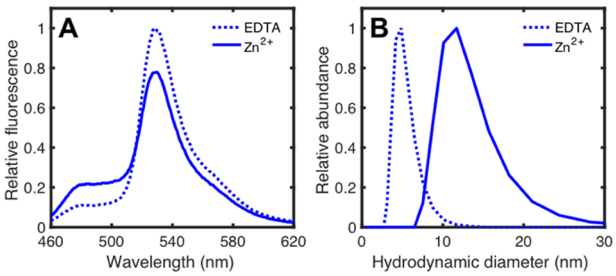

Figure 2. Upon binding to Zn^{2+}, ZifCV1.173 displays a decrease in FRET efficiency and an increase in size. (A) Representative emission spectra of ZifCV1.173 under 440 nm excitation in the presence of EDTA (dashed lines) and Zn^{2+} (solid lines). Spectra are scaled so that the value of 531 nm fluorescence in the presence of EDTA is one. The maximum and minimum FRET ratios, R_{max} and R_{min}, are calculated as the maximum and minimum ratios of the 531 nm fluorescence to 485 nm fluorescence intensities. (B) Representative DLS spectra of ZifCV1.173 in the presence of EDTA (dashed lines) and Zn^{2+} (solid lines).

the presence of Zn^{2+} (solid lines) and EDTA (dashed lines). ZifCV1.173 had an R_{max} of 9.2 ± 0.2 and an R_{min} of 3.7 ± 0.2, giving it a DR of 2.5 ± 0.1 based on eq 1, which closely matches the DR reported in HeLa cells. In contrast to most FRET sensors, which achieve R_{min} in their unbound forms and R_{max} in their bound forms, ZifCV1.173 showed an inverted response to Zn^{2+} binding, which is the same behavior that was reported in cells.[17] The inverted response suggests that in the presence of EDTA where the Zn^{2+} binding domain (ZBD) is unstructured, the FP domains are either in close proximity or are otherwise oriented for efficient FRET. Folding of the ZBD upon Zn^{2+} binding then creates separation between ECFP and cpVenus173 or alters their orientation resulting in reduced FRET efficiency.

To identify the molecular determinants of the large DR of the inverted-responding ZifCV1.173, we interrogated it using DLS and time-resolved fluorescence anisotropy. Figure 2B shows representative DLS spectra for ZifCV1.173. The hydrodynamic diameter in the presence of EDTA (dashed lines) was 5.2 ± 0.2 nm with a full width at half maximum (FWHM) of 3.5 ± 0.1 nm. In the presence of Zn^{2+} (solid lines), ZifCV1.173 underwent a large increase in size to 13.2 ± 0.4 nm with an increased FWHM of 7.5 ± 0.3 nm, suggesting more structural heterogeneity in this state. The change in hydrodynamic diameter of 8 nm upon Zn^{2+} binding could reflect a large increase in separation between ECFP and cpVenus173, explaining the large DR of ZifCV1.173. However, the DLS measurements result in observed diffusion coefficients, which require knowledge of shape to be directly related to size. Here, we assumed spherical shapes for our diffusing samples.[22] Although this is not necessarily a good approximation for multidomain molecules like ZifCV1.173, it is clear from Figure 2B that the Zn^{2+}-bound sensor diffused much more slowly than the Zn^{2+}-free sensor. To complement the translational diffusion changes of ZifCV1.173 in response to Zn^{2+} binding, we recorded fluorescence anisotropy decays of the donor fluorescence after donor excitation to capture rotational diffusion changes in response to Zn^{2+} binding. We measured a large increase in the rotational decay time for ZifCV1.173 upon Zn^{2+} binding (Figure S1), which is consistent with the size increase determined by DLS. Altogether, these data suggest that Zn^{2+} binding to ZifCV1.173 induced a large change in size and/or shape that resulted in a slowing of diffusion and a decrease in FRET between ECFP and cpVenus173.

The small hydrodynamic diameter of the Zn^{2+}-free state of ZifCV1.173 suggests that this state is compact, with the FP domains in close proximity. This makes sense given the large R_{max} of the sensor, which indicates efficient FRET between ECFP and cpVenus173. Additionally, ECFP and cpVenus173 are derived from *Aequorea victoria* GFP (hereafter, GFP), which dimerizes in the solution.[23,24] Therefore, ECFP and cpVenus173 may also associate when tethered by the relatively small ZBD. Indeed, considering the Zn^{2+}-free state of ZifCV1.173 as a 5.2 nm diameter sphere results in an effective FP concentration of >50 mM inside the sphere, which is nearly 3 orders of magnitude greater than the 0.1 mM K_D of GFP dimerization.[25] Moreover, a 5.2 nm sphere is hardly big enough to contain two FP domains of a single sensor (Figure S2), let alone the linkers and ZBD. Based on these geometric and affinity considerations, as well as the large R_{max} in the presence of EDTA, ECFP and cpVenus173 likely associate in the unbound form of ZifCV1.173.

Because we suspected an intramolecular association between the FP domains of the Zn^{2+}-free state of ZifCV1.173, we wondered if these domains interacted with a similar geometry to that of GFP dimers. We investigated this possibility by measuring the time-resolved fluorescence anisotropy of the FRET signal after donor excitation to determine the relative orientation between the transition dipole moments of ECFP and cpVenus173. Fluorescence anisotropy reflects the relative orientation of the excitation and emission transition dipole moments, and is described by eq 3, where r_0 is the initial anisotropy of the detected photons and θ_T is the transfer angle between transition dipole moments (illustrated in Figure S3).[26]

$$r_0(\theta_T) = \frac{3}{5}\cos^2(\theta_T) - \frac{1}{5} \quad (3)$$

In the case of FRET, exciting the donor and recording the anisotropy of the acceptor leads to an initial anisotropy that reflects the orientation between donor and acceptor transition dipole moments. This technique has been used to investigate FRET in several FP systems, including yellow fluorescent

DOI: 10.1021/acs.jpcb.9b02479
J. Phys. Chem. B 2019, 123, 3079−3085

protein (YFP) dimers,[27] a Ca^{2+} FRET sensor,[28] and a molecular crowding FRET sensor.[29]

Figure 3A shows representative FRET anisotropy decays of ZifCV1.173 after donor excitation. In the presence of Zn^{2+}

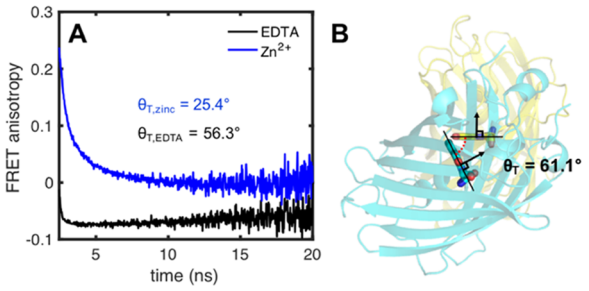

Figure 3. ECFP and cpVenus173 domains in the unbound form of ZifCV1.173 are oriented similarly to GFP molecules in the GFP dimer crystal structure. (A) Representative anisotropy decays of the FRET signal (515−569 nm) of ZifCV1.173 upon 440 nm excitation in the presence of EDTA (black) and Zn^{2+} (blue). (B) The crystal structure of GFP, (pdb: 1gfl) with two molecules in the unit cell oriented so that the angle between adjacent chromophores (rendered as sticks) can easily be seen. θ_T, calculated from the crystal structure, is 61.1° (dashed red arc). Lines are drawn through both chromophores to guide the eye.

(blue), r_0 was 0.24 ± 0.01 and decayed to zero at long times. However, in the presence of EDTA (black), r_0 was −0.01 ± 0.01 and remained negative even at long times, similar to observations of YFP dimers.[27] From eq 3, these r_0 values result in θ_T values between ECFP and cpVenus173 of 25.4 ± 0.9° in Zn^{2+} and 56.3 ± 0.4° in EDTA. One factor that would normally limit the straightforward estimation of θ_T from r_0 is the presence of donor fluorescence in the FRET emission window. However, because of the high R_{max} values of the sensor, the amount of donor fluorescence in the FRET emission window was negligible. The change in θ_T of 30.9° coupled with the large increase in hydrodynamic diameter from DLS suggests that ZifCV1.173 changed drastically in molecular configuration upon Zn^{2+} binding. Interestingly, θ_T of 56.3° in the unbound form of ZifCV1.173 closely matches θ_T between adjacent chromophores in the GFP dimer crystal structure (Figure 3B), which we calculated to be 61.1° (see Supporting Note).

Our observations that the unbound form of ZifCV1.173 had (1) a large R_{max}, suggestive of efficient FRET in its unbound form, (2) a small hydrodynamic diameter, and (3) a θ_T between the chromophores in ECFP and cpVenus173 that closely matches θ_T between GFP dimer chromophores, all point to a molecular configuration where ECFP and cpVenus173 are in close association in the unbound form of the sensor, in an orientation resembling the GFP dimer complex. To examine this possibility, we made mutations to the sensor that would alter the interaction between ECFP and cpVenus173 if they were indeed oriented similarly to the GFP crystal structure. We would then expect to see changes in the FRET efficiency between ECFP and cpVenus173, and thus the overall DR of the sensor.

To disrupt the hypothesized donor−acceptor interaction, we made the A206K mutation to the ECFP domain of ZifCV1.173. A206K disrupts the homodimerization of GFP,[30] so if ECFP and cpVenus173 associate at the same interface in ZifCV1.173, their interaction should be disrupted.

Representative emission spectra of this mutant sensor in the presence and absence of Zn^{2+} are shown in Figure 4A (red).

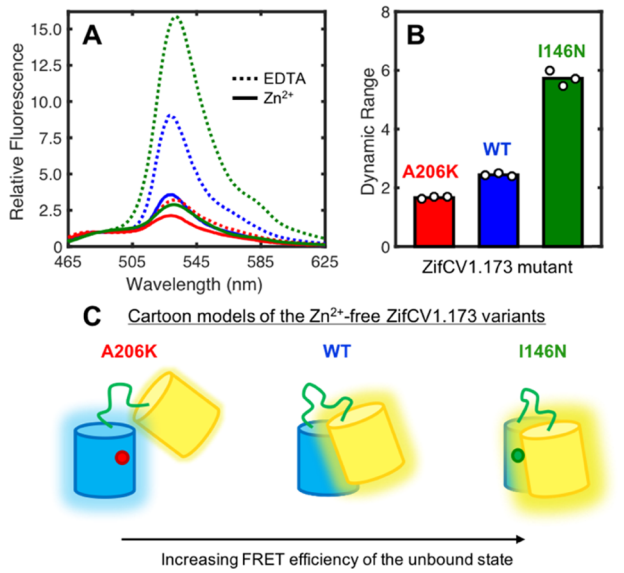

Figure 4. The dynamic range of ZifCV1.173 can be modulated by mutating the surface of ECFP. (A) Representative emission spectra of the three variants of ZifCV1.173 in the presence of EDTA (dashed lines) and Zn^{2+} (solid lines), colored according to the labels in panel (B). Spectra are scaled so that the 485 nm fluorescence intensity is one in all cases, which makes the 531 nm peak equal to either R_{max} or R_{min}. (B) Dynamic range measurements for all three variants of ZifCV1.173. The bars indicate the average of three measurements, whereas the individual measurements are shown as dots. (C) A cartoon model of the unbound forms of the ZifCV1.173 variants. ECFP and cpVenus173 are shown as blue and yellow cylinders, respectively, linked by the zinc binding domain in green. Red and green dots represent the A206K and I146N mutations, respectively.

Relative to wild type (WT) ZifCV1.173 (blue), the A206K variant had reduced R_{min} (1.9 ± 0.1) and R_{max} (3.2 ± 0.1) values, suggesting that the FRET efficiency between ECFP and cpVenus173 was reduced in both the bound and unbound forms of the A206K variant. However, the reduction in R_{max} was more pronounced (281%, relative to WT) than the reduction in R_{min} (200%).

To promote the hypothesized donor−acceptor interaction, we made the I146N mutation to the ECFP domain of ZifCV1.173. I146N increases the homodimerization tendency of ECFP from a K_D of 3 to 0.51 mM (see Figure S4 for a detailed explanation).[31] The emission spectra of the I146N mutant are shown in Figure 4A (green). In the presence of Zn^{2+}, R_{min} was 2.9 ± 0.1 (a 152% decrease relative to WT), and in the presence of EDTA, R_{max} was 15.8 ± 0.3 (a 176% increase relative to WT). From Figure 4A, it is clear that both these mutations caused greater changes in the FRET efficiencies of the unbound states (R_{max}) than the bound states (R_{min}). Interestingly, the A206K mutation, which we thought might disrupt the ECFP−cpVenus173 interaction, decreased the FRET efficiency of the unbound state. Conversely, the I146N mutation, which we thought might enhance the ECFP−cpVenus173 interaction, increased the FRET efficiency of the unbound state. Moreover, the observation that these GFP dimer-influencing mutations altered the FRET efficiency between ECFP and cpVenus173

DOI: 10.1021/acs.jpcb.9b02479
J. Phys. Chem. B 2019, 123, 3079−3085

suggests that the ECFP−cpVenus173 interface in the unbound form of ZifCV1.173 indeed resembles the GFP−GFP interface.

To understand how the intramolecular association between ECFP and cpVenus173 influenced the overall performance of ZifCV1.173, we measured the effect of the surface mutations on sensor DR (Figure 4B). Compared to the WT DR of 2.5, the A206K and I146N variants had DRs of 1.7 ± 0.1 and 5.7 ± 0.2, respectively. Interestingly, the dimer-disrupting mutation, A206K, decreased the DR, whereas the dimer-promoting mutation, I146N, increased the DR. This influence of intramolecular FP association on DR is similar to observations of other genetically encoded ion sensors.[7,32] From Figure 4A, it is clear that the DR changes were largely a result of the changes in R_{max}, which reflects the FRET efficiency of the Zn^{2+}-free sensor. Specifically, the 5.7 DR of the I146N mutant of ZifCV1.173 is one of the highest-reported DRs for an FP-based FRET sensor and is largely due to its high R_{max} of 15.8.

These observations led us to conclude that the intramolecular ECFP−cpVenus173 interaction in the unbound form of ZifCV1.173 is the dominant parameter in determining its DR. Figure 4C summarizes this idea and shows the hypothesized effect of the surface mutations. The A206K mutant of ZifCV1.173 had a reduced DR relative to WT, likely because A206K disrupted the ECFP−cpVenus173 interaction. This is supported by the decreased R_{max} of the A206K mutant sensor (Figure 4A) and the change in θ_T of the mutant sensor in the presence of EDTA (Figure S5). In contrast, the I146N mutant had an increased DR of 5.7, likely due to the promotion of the ECFP−cpVenus173 interaction by I146N. This is supported by the increase in R_{max} of the I146N mutant sensor (Figure 4A) and little change to θ_T (Figure S5).

To further test the accuracy of our cartoon model for the unbound form of the ZifCV1.173, we measured the apparent affinity of each sensor variant for Zn^{2+}. If the effect of the surface mutations is to alter the strength of the ECFP−cpVenus173 interaction, then one might expect the mutations to influence the apparent K_D for Zn^{2+}. Figure S6 shows Zn^{2+} titrations for all three ZifCV1.173 variants fit to eq 2. The apparent K_D values were 39.4 ± 3.8, 52.8 ± 4.7, and 64.2 ± 2.3 nM for the WT, A206K, and I146N variants, respectively. Relative to WT, both mutant sensors had a weaker apparent affinity for Zn^{2+}, although the effect was more pronounced for the I146N variant. Because we expected the I146N mutation to promote the ECFP−cpVenus173 interaction, it makes sense that the I146N variant had a weakened affinity: a higher Zn^{2+} concentration is required to disrupt the strengthened intramolecular FP association. However, the A206K variant did not show an increased affinity for Zn^{2+}, which might have been expected based on the hypothesized effect of the A206K mutation: reduced intramolecular FP association should make folding of the ZBD easier and thus give the sensor a greater apparent affinity for Zn^{2+}. That the apparent K_D values do not trend straightforwardly with sensor DR is likely a reflection of the fact that knowledge of the identity of the Zn^{2+}-bound state, in addition to that of the Zn^{2+}-free state, is necessary to fully rationalize these apparent affinities. However, the overall effect of these mutations on sensor affinity is relatively small compared to their effect on DR.

Although our experimental approach has proven valuable in identifying intramolecular FP association as a key determinant of the DR of these sensors, the effectiveness of surface mutations in promoting the formation of a compact, high FRET state and a higher DR has also been discussed in the context of other Zn^{2+} sensors and in protease sensors.[7,18−20,33] For example, Nguyen and Daugherty developed a cyan-yellow FRET pair, called CyPet-YPet, which is optimized for efficient FRET due to mutations to the FP domain surfaces that promote their intramolecular association.[20,33] However, even without any optimization of ECFP and cpVenus173 surface residues, the WT ZifCV1.173 adopts a compact intramolecular dimer-like conformation in the absence of Zn^{2+} with high FRET, similar to the CyPet-YPet pair. The formation of this compact state is likely due to the combination of two factors: (1) the relative orientation of ECFP and cpVenus173 compared to a differently permuted acceptor and (2) the relatively small size of the ZBD and linkers. These two factors allow the donor and acceptor domains of ZifCV1.173 to be in a favorable orientation for association with a high effective FP concentration due to the fact that the FP domains are tethered by only 38 amino acids (ZBD and linkers).

With this model of the Zn^{2+}-free state of ZifCV1.173, and a rationale for increasing DR, we made the same mutations to a related sensor, ZifCV1.157, to test the generalizability of our model. In ZifCV1.157, cpVenus173 is replaced by cpVenus157, causing the donor and acceptor FPs to have a different relative orientation (see Figure 1 and caption for details). The DR values of the ZifCV1.157 variants are shown in Figure 5A,

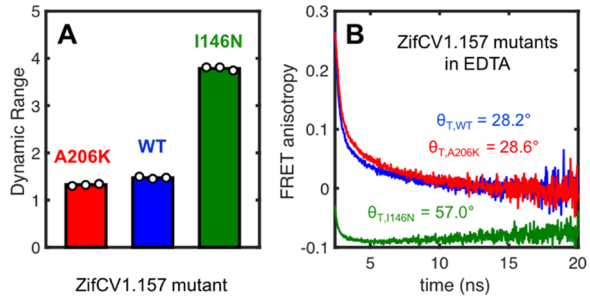

Figure 5. A206K and I146N mutations influence the dynamic range of ZifCV1.157 in a similar fashion to the mutations in ZifCV1.173. (A) Dynamic range measurements for all three variants of ZifCV1.157. The bars indicate the average of three measurements, whereas the individual measurements are shown as dots. (B) Representative FRET anisotropy decays (515−569 nm) after 440 nm excitation for the three ZifCV1.157 variants in the presence of EDTA, colored according to the bars in panel (A). Transfer angles, calculated from eq 3, are shown for each mutant.

where the A206K mutant had the lowest DR (1.3 ± 0.1), WT had a slightly higher DR (1.5 ± 0.1), and the I146N variant had a DR of 3.8 ± 0.1, nearly triple that of WT. Similar to the ZifCV1.173 variants, the DR changes in ZifCV1.157 were due to the greater variability in R_{max} compared to R_{min} (Figure S7). The R_{max} values of the ZifCV1.157 variants trended in the same order as those of the ZifCV1.173 variants (A206K < WT < I146N), suggesting that the same intramolecular donor−acceptor interaction was at play in the ZifCV1.157 variants. Additionally, FRET anisotropy decays in the presence of EDTA (Figure 5B) resulted in θ_T of 28.2 ± 0.3 and 28.6 ± 0.1° for the WT ZifCV1.157 and A206K mutant, respectively. However, the I146N mutant had a θ_T of 57.0 ± 0.3°, which closely matches that of the GFP dimer crystal structure (Figure 3B). Conversely, in the presence of Zn^{2+}, all three variants had similar θ_T values between 28.8° and 31.2° (Figure S8). The θ_T values for the unbound ZifCV1.157 variants suggest that unlike ZifCV1.173, which adopts the GFP dimer-like conformation in

DOI: 10.1021/acs.jpcb.9b02479
J. Phys. Chem. B 2019, 123, 3079−3085

its unbound form, cpVenus157 prevents ZifCV1.157 from adopting this same orientation. The unbound WT ZifCV1.157 may then resemble the configuration for the A206K mutant of ZifCV1.173 in Figure 4C, which explains why A206K had little effect on θ_T and R_{max} of ZifCV1.157 (Figures 5B and S7). However, I146N had a pronounced effect on the DR, θ_T, and R_{max} of ZifCV1.157, forcing the unbound sensor to adopt a configuration that resembled the GFP dimer complex and leading to highly efficient FRET (R_{max} = 15). Thus, the high FRET efficiency resulting from the intramolecular ECFP−cpVenus association provides the basis for this class of sensors to achieve a high DR.

The model that we have drawn for the unbound form of these Zif268-based sensors is reminiscent of the eCALWY class of Zn^{2+} FRET sensors, which also have inverted FRET responses due to surface modifications that stabilize the intramolecular association of donor and acceptor FP domains in the unbound state.[7] However, in the case of eCALWY and other inverted-responding FRET sensors, steady-state fluorescence anisotropy and size exclusion chromatography have often been used to infer the formation of intramolecular FP domain interactions, but the studies did not seek to measure the geometric parameters describing the structures of the compact ligand-free states.[7,18,33,34] Here, the combination of DLS and time-resolved fluorescence anisotropy allowed us to determine not only that the intramolecular FP domain interactions exist in the Zif268-based sensors, but that they cause the donor and acceptor FPs to associate with a similar orientation to the GFP dimer crystal structure. Moreover, our observation that the I146N mutation can force the unbound state of the sensors to adopt a compact, high FRET state even in the case of ZifCV1.157 where the FP domains are not optimally oriented for close association, suggests that I146N might be able to further enhance the DR of other FRET sensors that operate with a similar mechanism.

In all of the sensor variants analyzed here, the DR was dominated by the FRET ratio in the unbound state, R_{max}. However, the slight variations in R_{min} that can be seen in Figures 4A and S7 suggest that the mutations to the surface of the ECFP domain may have influenced the intra- or intermolecular dimerization tendency of the Zn^{2+}-bound form of the sensors as well. As a preliminary test of this hypothesis, we measured the DLS spectra of the ZifCV1.173 mutant sensors in the presence of Zn^{2+} to compare to the WT hydrodynamic properties reported in Figure 2B. Interestingly, the A206K mutation induced a decrease in hydrodynamic diameter of 3.8 nm relative to WT in the bound form of the sensor (Figure S9). Conversely, the I146N variant of ZifCV1.173 aggregated in the presence of Zn^{2+} at the relatively high sensor concentrations required for DLS measurements. This reduction in size of the A206K variant and aggregation of the I146N variant suggests that the bound form of these sensors might consist of intermolecular dimers (or higher order oligomers) that can be destabilized or stabilized by A206K or I146N, respectively, in much the same way that these mutations influence the intramolecular FP association in the Zn^{2+}-free state. The formation of intermolecular dimers in the presence of Zn^{2+} might also allow us to rationalize the effects of the surface mutations on apparent binding affinity. Ongoing work in our laboratory is focused on developing a molecular picture of the Zn^{2+}-bound form of these sensors so that we can fine tune the delicate balance between promoting intramolecular association of the FP domains while also reducing the tendency to form intermolecular dimers.

CONCLUSIONS

We have shown compelling evidence from DLS and time-resolved fluorescence anisotropy that the Zn^{2+}-free state of ZifCV1.173 is compact, with ECFP and cpVenus173 oriented similarly to GFP dimers. This results in a large R_{max}, which when coupled with the low R_{min} of the Zn^{2+}-bound state, leads to a large DR. Similar to what has been observed for other FRET sensors, the ECFP−cpVenus173 association could be rationally perturbed to manipulate the value of R_{max}, allowing us to control the sensor DR. We developed a model describing the influence of this intramolecular association on the overall sensor DR and used it to improve the DR of the closely related, poor performing ZifCV1.157 by nearly a factor of three. Our success in tuning sensor DR on the basis of our model highlights the value of careful biophysical characterization of FRET sensors and suggests that our experimental approach could provide similar insight into the mechanisms of other sensors.

ASSOCIATED CONTENT

Supporting Information

The Supporting Information is available free of charge on the ACS Publications website at DOI: 10.1021/acs.jpcb.9b02479.

Sequences of ZifCV1.157 and ZifCV1.173; donor anisotropy decays of ZifCV1.173; superposition of crystal structure 1gfl into a 5.2 nm sphere; visual representation of θ_T; close-up view of GFP dimer interface with ECFP overlaid; FRET anisotropy decays for ZifCV1.173 variants; Zn^{2+} titrations for ZifCV1.173 variants; emission spectra of ZifCV1.157 variants; FRET anisotropy decays for ZifCV1.157 variants; DLS spectra of ZifCV1.173 variants; details of θ_T calculation (PDF)

AUTHOR INFORMATION

Corresponding Author

*E-mail: rjimenez@jila.colorado.edu.

ORCID

Joshua D. Slocum: 0000-0002-8705-3054
Amy E. Palmer: 0000-0002-5794-5983
Ralph Jimenez: 0000-0002-8989-405X

Notes

The authors declare no competing financial interest.

ACKNOWLEDGMENTS

This work was supported by the NSF Physics Frontier Center at JILA (PHY 1734006 to R.J.) and NIH R01 GM084027 (to A.E.P). J.D.S. was supported by an NRC Postdoctoral Fellowship. We would like to thank the Anseth group at CU Boulder for allowing us to use their Malvern Zetasizer and Genevieve Park for generating the pBAD constructs of WT ZifCV.157 and WT ZifCV1.173. R.J. is a staff member in the Quantum Physics Division of the National Institute of Standards and Technology (NIST). Certain commercial equipment, instruments, or materials are identified in this paper to specify the experimental procedure adequately. Such an identification is neither intended to imply recommendation or endorsement by the NIST nor is it intended to imply that

DOI: 10.1021/acs.jpcb.9b02479
J. Phys. Chem. B 2019, 123, 3079−3085

the materials or equipment identified are necessarily the best available for the purpose.

REFERENCES

(1) Greenwald, E. C.; Mehta, S.; Zhang, J. Genetically Encoded Fluorescent Biosensors Illuminate the Spatiotemporal Regulation of Signaling Networks. *Chem. Rev.* **2018**, *118*, 11707−11794.

(2) Hellwig, N.; Plant, T. D.; Janson, W.; Schäfer, M.; Schultz, G.; Schaefer, M. TRPV1 Acts as Proton Channel to Induce Acidification in Nociceptive Neurons. *J. Biol. Chem.* **2004**, *279*, 34553−34561.

(3) Rupprecht, C.; Wingen, M.; Potzkei, J.; Gensch, T.; Jaeger, K. E.; Drepper, T. A Novel FbFP-Based Biosensor Toolbox for Sensitive in Vivo Determination of Intracellular PH. *J. Biotechnol.* **2017**, *258*, 25−32.

(4) Tsien, R. Y.; Miyawaki, A.; Llopis, J.; Heim, R.; McCaffery, J. M.; Adams, J. A.; Ikura, M. Fluorescent Indicators for Calcium Based on Green Fluorescent Proteins and Calmodulin. *Nature* **1997**, *388*, 882−887.

(5) Thestrup, T.; Litzlbauer, J.; Bartholomäus, I.; Mues, M.; Russo, L.; Dana, H.; Kovalchuk, Y.; Liang, Y.; Kalamakis, G.; Laukat, Y.; et al. Optimized Ratiometric Calcium Sensors for Functional in Vivo Imaging of Neurons and T Lymphocytes. *Nat. Methods* **2014**, *11*, 175−182.

(6) Qin, Y.; Dittmer, P. J.; Park, J. G.; Jansen, K. B.; Palmer, A. E. Measuring Steady-State and Dynamic Endoplasmic Reticulum and Golgi Zn^{2+} with Genetically Encoded Sensors. *Proc. Natl. Acad. Sci. U.S.A.* **2011**, *108*, 7351−7356.

(7) Vinkenborg, J. L.; Nicolson, T. J.; Bellomo, E. A.; Koay, M. S.; Rutter, G. A.; Merkx, M. Genetically Encoded FRET Sensors to Monitor Intracellular Zn^{2+} homeostasis. *Nat. Methods* **2009**, *6*, 737−740.

(8) Imamura, H.; Huynh Nhat, K. P.; Togawa, H.; Saito, K.; Iino, R.; Kato-Yamada, Y.; Nagai, T.; Noji, H. Visualization of ATP Levels inside Single Living Cells with Fluorescence Resonance Energy Transfer-Based Genetically Encoded Indicators. *Proc. Natl. Acad. Sci. U.S.A.* **2009**, *106*, 15651−15656.

(9) Hires, S. A.; Zhu, Y.; Tsien, R. Y. Optical Measurement of Synaptic Glutamate Spillover and Reuptake by Linker Optimized Glutamate-Sensitive Fluorescent Reporters. *Proc. Natl. Acad. Sci. U.S.A.* **2008**, *105*, 4411−4416.

(10) Forster, T. Zwischenmolekulare Energiewander-ung Und Fluoreszenz. *Ann. Phys.* **1948**, *437*, 55−75.

(11) Komatsu, N.; Aoki, K.; Yamada, M.; Yukinaga, H.; Fujita, Y.; Kamioka, Y.; Matsuda, M. Development of an Optimized Backbone of FRET Biosensors for Kinases and GTPases. *Mol. Biol. Cell* **2011**, *22*, 4647−4656.

(12) Nagai, T.; Yamada, S.; Tominaga, T.; Ichikawa, M.; Miyawaki, A. Expanded Dynamic Range of Fluorescent Indicators for Ca^{2+} by Circularly Permuted Yellow Fluorescent Proteins. *Proc. Natl. Acad. Sci. U.S.A.* **2004**, *101*, 10554−10559.

(13) Lelimousin, M.; Noirclerc-Savoye, M.; Lazareno-Saez, C.; Paetzold, B.; Le Vot, S.; Chazal, R.; Macheboeuf, P.; Field, M. J.; Bourgeois, D.; Royant, A. Intrinsic Dynamics in ECFP and Cerulean Control Fluorescence Quantum Yield. *Biochemistry* **2009**, *48*, 10038−10046.

(14) Rekas, A.; Alattia, J. R.; Nagai, T.; Miyawaki, A.; Ikura, M. Crystal Structure of Venus, a Yellow Fluorescent Protein with Improved Maturation and Reduced Environmental Sensitivity. *J. Biol. Chem.* **2002**, *277*, 50573−50578.

(15) Peisach, E.; Pabo, C. O. Constraints for Zinc Finger Linker Design as Inferred from X-Ray Crystal Structure of Tandem Zif268-DNA Complexes. *J. Mol. Biol.* **2003**, *330*, 1−7.

(16) Dittmer, P. J.; Miranda, J. G.; Gorski, J. A.; Palmer, A. E. Genetically Encoded Sensors to Elucidate Spatial Distribution of Cellular Zinc. *J. Biol. Chem.* **2009**, *284*, 16289−16297.

(17) Park, J. G.; Qin, Y.; Galati, D. F.; Palmer, A. E. New Sensors for Quantitative Measurement of Mitochondrial Zn^{2+}. *ACS Chem. Biol.* **2012**, *7*, 1636−1640.

(18) Lindenburg, L. H.; Hessels, A. M.; Ebberink, E. H. T. M.; Arts, R.; Merkx, M. Robust Red FRET Sensors Using Self-Associating Fluorescent Domains. *ACS Chem. Biol.* **2013**, *8*, 2133−2139.

(19) Hessels, A. M.; Chabosseau, P.; Bakker, M. H.; Engelen, W.; Rutter, G. A.; Taylor, K. M.; Merkx, M. EZinCh-2: A Versatile, Genetically Encoded FRET Sensor for Cytosolic and Intraorganelle Zn^{2+} Imaging. *ACS Chem. Biol.* **2015**, *10*, 2126−2134.

(20) Nguyen, A. W.; Daugherty, P. S. Evolutionary Optimization of Fluorescent Proteins for Intracellular FRET. *Nat. Biotechnol.* **2005**, *23*, 355−360.

(21) Pomorski, A.; Kochańczyk, T.; Miłoch, A.; Krężel, A. Method for Accurate Determination of Dissociation Constants of Optical Ratiometric Systems: Chemical Probes, Genetically Encoded Sensors, and Interacting Molecules. *Anal. Chem.* **2013**, *85*, 11479−11486.

(22) Edward, J. T. Molecular Volumes and the Stokes-Einstein Equation. *J. Chem. Educ.* **1970**, *47*, 261.

(23) Tsien, R. Y. The Green Fluorescent Protein. *Annu. Rev. Biochem.* **1998**, *67*, 509−544.

(24) Yang, F.; Moss, L. G.; Phillips, G. N., Jr. The Molecular Structure of Green Fluorescent Protein. *Nat. Biotechnol.* **1996**, *14*, 1246−1251.

(25) Phillips, G. Structure and Dynamics of Green Fluorescent Protein. *Curr. Opin. Struct. Biol.* **1997**, *7*, 821−827.

(26) Lakowicz, J. R. *Principles of Fluorescence Spectroscopy*, 3rd ed.; Springer Science+Business Media, 2006.

(27) Shi, X.; Basran, J.; Seward, H. E.; Childs, W.; Bagshaw, C. R.; Boxer, S. G. Anomalous Negative Fluorescence Anisotropy in Yellow Fluorescent Protein (YFP 10C): Quantitative Analysis of FRET in YFP Dimers. *Biochemistry* **2007**, *46*, 14403−14417.

(28) Borst, J. W.; Laptenok, S. P.; Westphal, A. H.; Kühnemuth, R.; Hornen, H.; Visser, N. V.; Kalinin, S.; Aker, J.; Van Hoek, A.; Seidel, C. A. M.; et al. Structural Changes of Yellow Cameleon Domains Observed by Quantitative FRET Analysis and Polarized Fluorescence Correlation Spectroscopy. *Biophys. J.* **2008**, *95*, 5399−5411.

(29) Currie, M.; Leopold, H.; Schwarz, J.; Boersma, A. J.; Sheets, E. D.; Heikal, A. A. Fluorescence Dynamics of a FRET Probe Designed for Crowding Studies. *J. Phys. Chem. B* **2017**, *121*, 5688−5698.

(30) Zacharias, D. A.; Violin, J. D.; Newton, A. C.; Tsien, R. Y. Partitioning of Lipid-Modified Monomeric GFPs into Membrane Microdomains of Live Cells. *Science* **2002**, *296*, 913−916.

(31) Espagne, A.; Erard, M.; Madiona, K.; Derrien, V.; Jonasson, G.; Lévy, B.; Pasquier, H.; Melki, R.; Mèrola, F. Cyan Fluorescent Protein Carries a Constitutive Mutation That Prevents Its Dimerization. *Biochemistry* **2011**, *50*, 437−439.

(32) Kotera, I.; Iwasaki, T.; Imamura, H.; Noji, H.; Nagai, T. Reversible Dimerization of *Aequorea Victoria* Fluorescent Proteins Increases the Dynamic Range of FRET-Based Indicators. *ACS Chem. Biol.* **2010**, *5*, 215−222.

(33) Vinkenborg, J. L.; Evers, T. H.; Reulen, S. W. A.; Meijer, E. W.; Merkx, M. Enhanced Sensitivity of FRET-Based Protease Sensors by Redesign of the GFP Dimerization Interface. *ChemBioChem* **2007**, *8*, 1119−1121.

(34) Malisauskas, M.; van de Graaf, S. F. J.; Sips, T.; Merkx, M.; Lindenburg, L. H.; van Oppen, L.; Wijnands, S. P. W. Quantifying Stickiness: Thermodynamic Characterization of Intramolecular Domain Interactions To Guide the Design of Förster Resonance Energy Transfer Sensors. *Biochemistry* **2014**, *53*, 6370−6381.

DOI: 10.1021/acs.jpcb.9b02479
J. Phys. Chem. B 2019, 123, 3079−3085